HHS Public Access

Author manuscript

Glia. Author manuscript; available in PMC 2024 September 01.

Published in final edited form as:

Glia. 2023 September ; 71(9): 2196–2209. doi:10.1002/glia.24387.

Ablation of Argonaute 2 in Schwann cells accelerates the progression of diabetic peripheral neuropathy

Baoyan Fan[1], **Michael Chopp**[1,2], **Yi Zhang**[1], **Xinli Wang**[1], **Amy Kemper**[3], **Zheng Gang Zhang**[1], **Xian Shuang Liu**[1]

[1]Department of Neurology, Henry Ford Health System, Detroit, MI 48202

[2]Department of Physics, Oakland University, Rochester, MI 48309

[3]Department of Pathology, Henry Ford Hospital, Detroit, MI, 48202.

Abstract

Schwann cells (SCs) form myelin and provide metabolic support for axons, and are essential for normal nerve function. Identification of key molecules specific to SCs and nerve fibers may provide new therapeutic targets for diabetic peripheral neuropathy (DPN). Argonaute2 (Ago2) is a key molecular player that mediates the activity of miRNA-guided mRNA cleavage and miRNA stability. Our study found that Ago2 knockout (Ago2-KO) in proteolipid protein (PLP) lineage SCs in mice resulted in a significant reduction of nerve conduction velocities and impairments of thermal and mechanical sensitivities. Histopathological data revealed that Ago2-KO significantly induced demyelination and neurodegeneration. When DPN was induced in both wild-type and Ago2-KO mice, Ago2-KO mice exhibited further decreased myelin thickness and exacerbated neurological outcomes compared with wild-type mice. Deep sequencing analysis of Ago2 immunoprecipitated complexes showed that deregulated miR-206 in Ago2-KO mice is highly related to mitochondrial function. In vitro data showed that knockdown of miR-200 induced mitochondrial dysfunction and apoptosis in SCs. Together, our data suggest that Ago2 in SCs is essential to maintain peripheral nerve function while ablation of Ago2 in SCs exacerbates SC dysfunction and neuronal degeneration in DPN. These findings provide new insight into the molecular mechanisms of DPN.

Graphical Abstract

The ablation of Argonaute2 in Schwann cells induces mitochondrial dysfunction and exacerbates the demyelination and neurodegeneration of sciatic nerves, which leads to peripheral neuropathy.

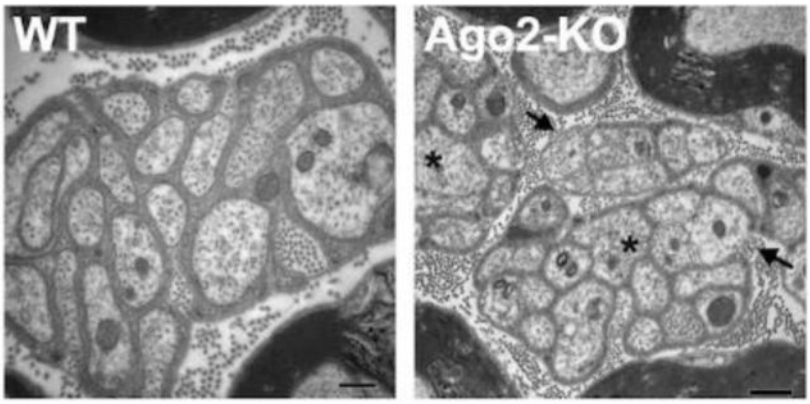

Keywords

Schwann cells; Argonaute2; miRNA; diabetic peripheral neuropathy; mitochondria

Introduction

Diabetic peripheral neuropathy (DPN) is a major complication of diabetes mellitus. It is estimated that by 2050, about 3.2 billion individuals will have diabetes, and half of them will develop DPN[1]. The progression of painful DPN increases the chance of ulcers and amputations as well as the cost of care[2]. To date, therapy options for DPN patients include diet intervention and pain management, but these treatments are not sufficient to ameliorate the major symptoms of the disease[3]. Recent data suggest that chronic hyperglycemia targets Schwann cells (SCs) and that severe DPN cases exhibit features of demyelination[4].

SCs form myelin and provide metabolic support for axons[4]. Myelin maintains the saltatory conduction of action potentials along neurons[5]. SCs regulate the cytoskeletal properties of axons via the secretion of growth factors and hormones, including brain-derived neurotrophic factor (BDNF), nerve growth factor (NGF), neurotrophin receptor p75 ($p75^{NTR}$), and glial-derived neurotrophic factor (GDNF)[6]. These factors promote axon growth and protect neurons from programmed cell death[4]. In addition, SCs are directly involved in axonal regeneration in DPN. Under hyperglycemic conditions, SCs dedifferentiate to an immature phase and support axonal regeneration[7].

In diabetic individuals, increased glucose levels lead to the activation of poly (ADP-ribose) polymerase and hexosamine pathways, which thereby increase reactive oxygen species (ROS) accumulation and inflammation, leading to mitochondrial dysfunction[8,9]. The role of axonal mitochondria in the progression of DPN has been widely studied[8]. However, the involvement of SC mitochondria in peripheral nerve disorders remains largely unknown. Of note, abnormal mitochondria in DPN patients often localize to SCs[10]. SCs are vulnerable to oxidative stress because of their large population of mitochondria, and the latter is both the source and target of ROS. ROS promotes outer mitochondrial membrane permeability, mitochondrial depolarization, and the release of pro-apoptotic factors[11]. Viader et al. reported that SC-specific mitochondria dysfunction could cause axonal degeneration[12].

Understanding how mitochondrial dysfunction in SCs contributes to DPN progression may advance the development of DPN therapy.

Recent publication revealed the involvement of microRNA (miRNA) in the development and progression of DPN[13]. Deregulation of miRNAs has been reported in the circulation as well as in the peripheral nervous tissues of diabetic patients[14]. Several miRNAs, including miRNA-1, −9, -sc8, −148, −210, −132, and −182, were confirmed to be involved in SC migration and proliferation in a mouse model of DPN[15]. As miRNA generally inhibits the translation of target mRNAs by RNA silencing, it is reasonable to hypothesize that the dysregulation of miRNAs may contribute to the suppression of proteins that support the function of the peripheral nervous system (PNS). Mature miRNAs function via loading into the miRNA-induced silencing complex (miRISC), and they direct the RISC to specific mRNA targets and inhibit their translation[16]. Ago2, the core component of miRISC, mediates mRNA cleavage or translational inhibition in mammals[16]. Circulating miRNAs can be released in complexes with Ago2, thereby enhancing the stability of cell-free miRNAs[17]. Deregulation of Ago2 is related to many disorders such as stress, angiogenesis, tumorigenesis, and hypoxia diseases[18,19], but the role of Ago2 and how its expression is regulated in DPN have not been well studied. Myelin proteolipid protein (PLP) is a component of the SC myelin sheath. In the present study, we used a tamoxifen-inducible PLP-Cre driver mouse line to test the potential role of Ago2 within SCs in the development of DPN.

Materials and Methods

Animals

All experimental procedures were approved by the Institutional Animal Care and Use Committee of Henry Ford Hospital, and were performed according to NIH Guidelines for the Care and Use of Laboratory Animals.

B6.Cg-Tg(Plp1-cre/ERT)3Pop/J mice (PLP-CreER^{T2}, stock#: 005975), B6.129P2(129S4)-*Ago2*$^{tm1.1Tara}$/J mice (Ago2 floxed, stock#: 016520), and B6.Cg-*Gt(ROSA)26Sor*$^{tm14(CAG-tdTomato)Hze}$/J mice (Rosa-TdTomato reporter, stock#: 007914) mice were purchased from Jackson lab. We crossed PLP-CreER^{T2} mice with Ago2 floxed mice and generated PLP-specific Ago2 KO mice (Ago2-KO). To trace Ago2-KO cells, the Ago2-KO mice were crossed with Rosa-TdTomato reporter mice and thereby obtained *PLP-CreER*^{T2}*; Ago2*$^{flox/flox}$ Tomato mice in which PLP-expressing cells with Ago2-KO can be traced utilizing TdTomato, which is a marker detected by the antibody against RFP. The wild-type (WT) control mice were generated by crossing PLP-CreER^{T2} mice with Rosa-TdTomato reporter mice.

The deletion of Ago2 was induced by intraperitoneal administration of tamoxifen (180mg/kg/d, Sigma-Aldrich, St. Louis, MO) for five consecutive days in male Ago2-KO mice at the age of 10-weeks. Tamoxifen was dissolved in 9:1 v/v sunflower seed oil (MilliporeSigma) and absolute ethanol. Tamoxifen-treated male WT mice of the same age were used as the control.

To induce DPN, after five days of tamoxifen administration, WT and Ago2-KO mice were fed by 60-kcal% high-fat diet (HFD, D12492; Research Diets) for 3 months and streptozotocin (STZ, 50mg/kg, MilliporeSigma) was administered daily for 5 consecutive days starting at 2 months after the initial HFD feeding. Electrophysiological and neurological tests were performed monthly for 3 months starting 1 month after termination of tamoxifen. Mitochondrial function, transmission electron microscopy (TEM), miRNA measurements, and immunohistochemistry were analyzed at 3 months after termination of tamoxifen injection.

Electrophysiology measurements

Sciatic nerve conduction velocity was assessed as previously described[20]. The tested mouse was anesthetized with 2% isoflurane and electrodes were placed at the ankle and sciatic notch, respectively, on the right side. An isolated pulse stimulator (Model 2100, A-M Systems, Sequim, WA, USA) was placed on the right front paw to deliver single square wave current pulses. Motor nerve conduction velocity (MCV) and Sensory nerve conduction velocity (SCV) were calculated according to our previous reports[20,21].

Measurement of thermal sensitivity

To examine the sensitivity of mice to thermal stimuli, a thermal stimulation meter (IITC model 336 TG; IITC Life Science, Woodland Hills, CA) was used to perform plantar and tail flick tests. The tested mice were separately placed on a glass surface, and the heat stimulator was set directly beneath the plantar surface of the hind paw or the tip of tail. The withdrawal latency in response to the radiant heat was recorded. For the plantar test, the heating intensity was set at 15% intensity, and the cut-off time was set at 30 sec. For the tail-flick test, the heating intensity was set at 40% and the cut-off time at 10 sec. Three readings were taken with 15 min intervals for each mouse[20].

Tactile allodynia test

To examine the sensitivity to mechanical stimuli, mice were placed on a net and the Von Frey filaments (forces ranging from 0.02 to 1.4 g, Stoelting) were applied to the plantar skin of the left hind paw using the pressure that caused the filament to buckle. The withdrawal in response to each stimulus was recorded and a 50% paw withdrawal threshold was calculated according to a published formula[22].

Myelin sheath staining

The sciatic nerve samples were cut into 2-μm thick semi-thin sections, as previously described[20,23]. The sections were stained with 1% toluidine blue. Image analysis was performed under a 100x objective of a light microscope (Olympus). The diameters of myelinated and unmyelinated fibers were measured. The g-ratio was calculated as axon diameter/fiber diameter.

Reactive oxygen species (ROS)

ROS was measured using OxiSelect™ In Vitro ROS/RNS Assay Kit (Cell Biolabs). Sciatic nerves were homogenized in PBS on ice. The suspension was centrifuged at 10,000 g for

5 min to remove insoluble particles, and 50μl of the supernatant was added to wells of a 96-well plate. 50μL of Catalyst was added to each well and incubated for 5 min at room temperature. 100 μL of DCFH solution was then added to each well and incubated for 30 min at room temperature in dark. The fluorescence was read using a fluorescence plate reader at 480 nm/ 530nm.

Mitochondrial DNA (mtDNA) quantitation

Total DNA from each sciatic nerve sample was isolated using Qiagen DNeasy Blood and Tissue Kit according to the manufacturer`s manual. mtDNA was measured using NovaQUANT Mouse Mitochondrial to Nuclear DNA Ratio Kit (Novagen). SYBR Green qPCR, the reaction mix containing 11.5 μL 2xRT^2 SYBR Green Mastermix and 11.5 μL of DNA were incubated at 95°C for 10min followed by 40 cycles of 95°C for 15 secs and 60 °C for 1 min. Relative quantities were calculated as $(2^{Ct(trLEV)-Ct(BECN1)}+2^{Ct(12s)-Ct(NEB)})/2$.

Mitochondrial membrane potential (Δψm)

Mitochondrial membrane potential was measured using MITO-ID Membrane potential cytotoxicity kit (Enzo life sciences). Sciatic nerves were homogenized in PBS on ice and centrifuged at 10,000g for 5 min at 4 °C. 100 μL of the supernatant was then added to wells of the microplate and added 100 μL of MP dye loading solution. The microplate was incubated for 30 min at room temperature in the dark. The fluorescence was read with a fluorescence plate reader at 490 nm/ 590nm.

ATP

ATP was measured using an ATP Colorimetric/Fluorometric Assay Kit (BioVision). Sciatic nerve tissues (10 mg) were lysed in 100 μL of ATP Assay Buffer. Deproteinized tissue homogenate was obtained using a 10 kDa Spin Column. Add 50 μl of sample to a 96-well plate. The volume was adjusted to 50 μl/well with an ATP Assay Buffer.

RNA immunoprecipitation (RIP)

RIP was performed using Magna RIP kit (MilliporeSigma) Ago2 antibody (Abcam) following the manufacturer’s instruction. Sciatic nerve tissue was lysed and incubated with magnetic protein A/G beads precoated with Ago2 antibody at 4°C overnight. The protein was digested with Proteinase K. The immunoprecipitated RNA was isolated for miRNA sequencing.

MiRNA sequencing

RNA samples were quantified using Nanodrop and qualified by agarose gel electrophoresis. RNA-seq library preparation, including procedures of RNA fragmentation, random hexamer primed first-strand cDNA synthesis, dUTP based second-strand cDNA synthesis, end-repairing, A-tailing, adaptor ligation, and library PCR amplification was performed using Illumina kits. The prepared RNA-seq libraries were qualified using Agilent 2100 Bioanalyzer and quantified by qPCR absolute quantification method. The sequencing was performed using Illumina Hiseq 4000. Hierarchical Clustering was used to analyze gene expression data. The heatmap was generated using significant differentially expressed genes.

Immunohistochemistry

Under anesthesia (ketamine, 50 mg/kg MilliporeSigma), animals were perfused with saline and followed with 4% paraformaldehyde. Peripheral nerve tissues were removed for dehydration and fixed in 4% paraformaldehyde overnight and immersed in 30% sucrose solutions for 5 days or until they sank to the bottom of the container. Then tissues were embedded in optimal cutting temperature (OCT) compound (Sakura Finetek), snap-frozen, and cut into 20-μm sections. The sections were blocked using 3% BSA and incubated with primary antibodies overnight at 4°C, followed by secondary antibodies incubation at a concentration of 1:300. Nuclei were counterstained with DAPI (1:10,000; Vector Laboratories). Images were taken in five random view fields per section. 1-in-10 series of sections were stained for each animal. The following primary antibodies used in the study include: chicken anti-red fluorescent protein (anti-RFP; 1:200; Rockland Antibodies & Assays), rabbit anti-myelin basic protein (MBP, 1:200; DAKO), rabbit anti-PGP9.5 (1:1000; Millipore), and mouse anti-neurofilament 200 (NF200, 1:200; MilliporeSigma).

$PGP9.5^+$ nerve fiber in the dermis within a 50-μm radius from the epidermal/dermal junction was measured, and the number of $PGP9.5^+$ nerve fibers with a cross-sectional area of ≤ 20 μm^2 was counted. Data are presented as nerve fiber density calculated based on a published formula[24]. The percentage of GAP43/NF200-colabeled cells was counted in four fields that were randomly chosen in sciatic nerves under 20× magnification of the fluorescent microscope.

Myelin sheath staining

Axonal caliber and myelin thickness were measured on semi-thin transverse sections (2-μm thick) stained with 1% toluidine blue, and three semi-thin sections per mouse were analyzed. For morphometric analysis of sciatic nerves, three sections spaced at 60 μm interval for each staining per mouse were used for analysis. Three fields of view per section were randomly imaged under a 100x oil immersion objective (BX40; Olympus Optical Co. Ltd) via the MCID system. Myelinated fiber diameter, axon diameter, and myelin sheath thickness were measured. To measure g-ratio and axonal diameter, the dense inner and outer impactive myelin sheaths were measured while the axonal diameter was outlined and measured. Then, g-ratio was calculated. At least 50–100 myelinated fibers were measured per animal[25–27]. Scatter plot graphs display g-ratio (y-axis) in relation to axon diameter (x-axis) of the individual fiber. All analyses were conducted by an examiner who was blinded to the identity of the samples being studied.

Western blot

Samples were lysed with RIPA buffer supplemented with 1% proteinase and centrifuged at 12000g for 15min to remove cell debris. Protein concentration in supernatant was determined using BCA assay (Thermo Fisher Scientific). 50μg of total protein from each sample was separated by SDS-PAGE and transferred to nitrocellulose membranes. After blocking, the membranes were incubated with the following antibodies: anti-β-actin (1: 5000; Abcam), anti-Ago2 (1:1000; Abcam), anti-myelin protein zero (MPZ, 1:1000; Abcam), anti-myelin basic protein (MBP, 1:1000; Abcam), anti-CNPase (1:500; MilliporeSigma), anti-mitofusin 1 (MFN, 1:500; Abcam), anti-dynamin-related protein

1 (DRP1, 1:500; Abcam), anti-fission 1 protein (FIS1, 1:1000; Abcam), anti-Advanced Glycation Endproducts (RAGE, 1:1000; R&D Systems), anti-NF-KB, p65 subunit (1:500, MilliporeSigma), and anti-Cleaved Caspase-3 (1:1000; Cell signaling technology). After incubation with secondary antibodies, the signals were visualized by enhanced ECL substrate (Thermo Fisher Scientific)

Transmission electron microscopy (TEM)

Sciatic nerves were dissected and fixed in 3% glutaraldehyde overnight and in 1% osmium tetroxide overnight at 4°C. Then, tissues were dehydrated in graded alcohols and embedded in epoxy, and cut into 1μm sections. Sections were stained with uranyl acetate and lead citrate. Images were taken under the transmission electron microscope (JEM-1500Flash, JEOL).

DRG neuron culture

Mice were perfused with saline and euthanized. DRGs were isolated and incubated with 0.125% collagenase (Worthington Biochemical Corp, Lakewood, NJ, USA) at 37 °C for 40 min followed by 0.25% trypsin (Worthington Biochemical Corp) for 30 min. The digestion was stopped with an equal volume of FBS and DRG neurons were mechanically triturated with a Pasteur pipette. The cell suspension was filtered through a 70-μm cell strainer (Thermo Fisher Scientific) and centrifuged to pellet the DRG neurons at 160g for 10 min. A microfluidic culture device (Cat# SND450, Xona Microfluidics, Temecula, CA) was used. The microfluidic device contained 450 μm long microgrooves that connected soma and axonal compartments and allowed only distal axons to grow into the axonal compartment. Briefly, culture dishes (35 mm, Corning) were coated with 0.5mg/ml poly-D-lysine (MilliporeSigma) at 37 °C for 2h followed by 1% lamin (Gibco) at 37 °C for 1h. Then, chambers were affixed to coated culture dishes. The primary DRG neurons were plated at a density of 6×10^5cells/device in growth media containing neurobasal medium (Invitrogen), nerve growth factor (50 ng/ml, MilliporeSigma), 2% B-27 supplement (Invitrogen), 1% GlutaMax (Invitrogen), and 1% antibiotic-antimycotic (Invitrogen). To purify the DRG neurons, DRG neurons were treated with 40μM FUDR (Sigma-Aldrich) for 3 days to inhibit the growth of glial cells, in which the purity of neurons at 99% could be achieved[28]. Immunofluorescent staining was conducted and axons were measured as previously described[29]. Briefly, a monoclonal antibody against phosphorylated neurofilament heavy protein (pNFH) (1:500; SMI31, Covance) was used. The length of the 15 longest axons in each chamber was measured using the MCID system.

Culture and transfection of Schwann cells

A mouse Schwann cell line was purchased from ScienCell (Cat. No. 1700–57), cultured in Schwann cell medium (ScienCell, Cat. No. 1701) supplemented with 5 ml of Schwann cell growth supplement (SCGS, Cat. No. 1752), 5 ml of Antibiotic solution (P/S, Cat. No. 0503), and 5% fetal bovine serum (FBS, Cat. No. 0025), and maintained at 37°C and 5% CO_2. To examine the effects of miR-206 on mitochondrial function, Schwann cells were transfected with a miR-206 inhibitor (miRIDIAN microRNA Mouse mmu-miR-206–3p inhibitor, IH-310462–07-0002) or an inhibitor negative control (NC, miRIDIAN microRNA Hairpin

Inhibitor Negative Control, IN-001005–01-05) using electroporation (Lonza Nucleofector device, program O01).

Statistical analysis

Data are presented as mean ± standard (SD). GraphPad Prism software (GraphPad Software Inc., CA, USA) was used for statistical analyses. Statistical significance was determined using nonparametric one-way analysis of variance (ANOVA) followed by the Tukey post hoc test, performed for multiple group comparisons and two-tailed Student's t-tests for two-group comparisons. A value of $p<0.05$ was taken as significant. Quantification was performed from at least three independent experiments.

Results

Ago2-KO mice display sciatic nerve dysfunction

Genotyping verified the construction of Ago2-KO mice (Fig. 1A). To activate the Cre-recombinase, the Ago2-KO or Ago2 reporter mice were treated with tamoxifen (Fig. 1B). Western blot analysis verified the knockdown of Ago2 in sciatic nerves compared to WT mice (Fig. 1C). To examine the effect of ablation of Ago2 in PLP lineaged–SCs on peripheral nerve function, we measured the peripheral neurological functions in Ago2-KO mice. The electrophysiological recording showed that Ago2-KO mice exhibited a significant reduction of motor and sensory conduction velocity (MCV and SCV) by 13.6% and 10.4%, respectively, three months after Ago2-KO compared with WT mice (Fig. 1D-E). At the same time, thermal and mechanical response latencies measured by plantar test, tail-flick test, and Von Frey test were significantly increased in Ago2-KO mice, compared with WT mice (Fig. 1F-H), indicating that ablation of Ago2 in SCs contributes to the development of peripheral neuropathy.

Ago2-deficient SCs fail to myelinate peripheral nerves

SCs are responsible for myelin production, which contributes to axonal protection and allows for efficient action potential transmission[307]. We employed toluidine blue staining to examine the change in myelination. As shown in Fig. 2A, the nerve fibers of WT mice were dense and myelinated, which is consistent with other studies[25–27]. The Ago2-KO mice showed substantially decreased myelin thickness and axon diameter (Fig. 2B-D, Table 1). Approximately ~7% of axons showed the myelin degenerating defect and ~12% of axons showed signs of degeneration (Fig 2A). The proportion of nerve fibers with a diameter of >8 μm was lower in Ago2-KO mice than those in WT mice (Fig. 2B). To analyze the thickness of myelination, we measured the g-ratio in Ago2-KO mice, which is the ratio of the inner versus outer layer diameter of the myelin sheath, with a lower g-ratio representing a larger degree of myelin per axon[31]. Our data showed that the average g-ratio was significantly increased in Ago2-KO mice compared WT mice (Table 1). When g-ratio was plotted versus axon caliber, there was a steepening in the regression line between two groups (Fig. 2E), indicating a reduction of myelin per axon in Ago2-KO mice.

Moreover, double immunostaining analysis revealed that Ago2-KO significantly decreased the numbers of double immunopositive PLP^+/MBP^+ Schwann cells or NF200+ nerve fibers

with PLP$^+$ Schwann cells (PLP$^+$/NF200$^+$) by 21.2% and 15.6%, respectively (Fig. 2F-I). In line with immunostaining, Western blot analysis demonstrated that the expression of myelin proteins including MBP, CNPase, and MPZ in the peripheral nerves of Ago2-KO mice were significantly decreased (Fig. 2J-K). These data suggest that deletion of Ago2 in SCs induces demyelination in sciatic nerves.

Ablation of Ago2 in SCs exacerbates DPN

Using high-fat diet in combination with a low dose of STZ, we induced DPN in both WT and Ago2-KO mice (Fig. 1D). We found that three months after HFD/STZ administration, WT mice developed DPN, whereas Ago2-KO mice developed DPN early starting at 2 months after HFD/STZ administration (Fig. 1D-H). Additionally, compared to WT+HFD/STZ mice, Ago2-KO+HFD/STZ mice developed severe DPN in which MCV and SCV were decreased by 9.5% and 11.1%, respectively (Fig. 1D-E). Data from the plantar test, tail-flick test, and Von Frey test showed that thermal and mechanical stimuli thresholds of Ago2-KO+HFD/STZ mice were markedly increased respectively (Fig. 1F-H). Moreover, compared to WT+HFD/STZ mice, Ago2-KO+HFD/STZ mice showed further augmentation of neurologic deficits from 2 months to 3 months after HFD/STZ administration in which MCV and SCV were further decreased by 13.7% and 11.7%, respectively, (Fig. 1D-E), the latency to heat stimuli was significantly 32.5% higher in plantar and 40.6% in tail, and mechanical sensitivity was 25.5% lower (Fig. 1F-H).

Next, we analyzed the morphometric changes in the peripheral nerves of HFD/STZ-treated mice. Analysis of toluidine-blue stained sciatic nerve sections demonstrated that diabetic WT mice showed a significant reduction in sciatic nerve fiber diameter and myelin sheath thickness, and a significant increase in g-ratio (Fig. 3A, 3E, Table 1). Moreover, the axonal diameter and myelin thickness were decreased by 31.6% and 14.3%, respectively, in Ago2-KO+HFD/STZ mice compared with WT+HFD/STZ group (Fig. 3C-D), indicating Ago2 KO enhanced the impairment of myelination. Furthermore, double immunofluorescent staining showed that WT+HFD/STZ mice exhibited a reduction of MBP positive myelination compared with WT mice (24.3±5.4 cells/100 μm^2 vs 42.2±2.4 cells /100 μm^2, $p<0.01$). Ago2-KO+HFD/STZ mice showed further demyelination compared with WT+HFD/STZ mice (5.7±1.2 cells/100 μm^2 vs 24.3±5.4 cells/100 μm^2, $p<0.001$. Fig. 3F-I), which was consistent with the data of Western blot analysis (Fig. 2J-K). Collectively, these data suggest that the knockout of Ago2 in SCs of diabetic mice promotes the development of neuropathy by enhancing diabetes-induced sciatic nerve demyelination.

Ablation of Ago2 in SCs disrupts small nerve fiber reinnervation

Intraepidermal nerve fibers (IENFs) consist predominantly of C small fibers, and the damage to these sensory nerve fibers can cause hypoesthesia and hyperalgesia[328]. Our data showed that dermal tissues obtained from Ago2-KO mice exhibited a significant reduction of IENF density assayed by the number of PGP9.5 positive fibers (31±4 fibers/mm in Ago2-KO mice vs 42±5 fibers/mm in WT mice, $p<0.01$. which is specific to all types of efferent and afferent peripheral nerve fibers, compared with WT mice (Fig. 4A-B). Also, our data showed the amount of co-expressing growth-associated protein 43 (GAP43)$^+$, a neuronal membrane protein involved in axonal growth and regeneration[33], with NF200$^+$ sciatic nerves, was

significantly lower in Ago2-KO mice than that in WT mice. Under the HFD/STZ induction, Ago2-KO mice exhibited further reduction of $GAP43^+/NF200^+$ nerve fibers (Fig 4C, D). Furthermore, we examined the bundles of unmyelinated axons in the sciatic nerves of WT and Ago2-KO mice. TEM assay demonstrated that in WT mice, C-fibers were individually partitioned by extensions of SC cytoplasm and grouped into Remak bundles (Fig. 4E). In contrast, abnormally differentiated Remak bundles were observed in Ago2-KO mice (Fig. 4E). The abnormalities included poorly segregated axons (Fig. 4E, marked with asterisks) and absent or thinned SC ensheathment (marked with arrows), which lead to the exposure of the axon to the endoneurium (Fig. 4E). These results suggest that Ago2 regulates the ensheathment of axons in non-myelinating Schwann cells.

To further examine the effect of ablation of Ago2 in PLP-SCs on DRG neurons, we measured axonal growth of primary DRG neurons cultured in a microfluidic device[34]. DRG neurons harvested from Ago2-KO mice exhibited a considerable reduction of axonal growth compared to the DRG neurons from WT mice (Fig. 4F-G). These data suggest that Ago2-KO in SCs affects axonal growth of DRG neurons.

Ago2 ablation in SCs causes mitochondrial dysfunction

Mitochondria are critical regulators in the development and maintenance of peripheral nerves. The impaired mitochondria exhibit mtDNA damage and reduced mitochondrial membrane potential ($\Delta\psi m$)[359]. We measured the mtDNA and $\Delta\psi m$ in sciatic nerve tissues. In Ago2-KO mice, mtDNA and $\Delta\psi m$ were 42% and 29% lower, respectively, compared with those in WT mice (Fig. 5A-B). In the sciatic nerves of Ago2-KO+HFD/STZ mice, the two parameters were 48% and 53% lower than those of WT+HFD/STZ mice (Fig. 5A-B). Axonal regeneration requires high consumption of mitochondrial-derived ATP[30]. We measured the content of ATP in sciatic nerves. In Ago2-KO mice, ATP content was significantly decreased compared with that in WT mice by 26%. In diabetic WT+HFD/STZ mice ATP was decreased by 56% compared to non-diabetic WT mice, and ablation of Ago2 further decreased ATP by 29% (Fig. 5C).

To further examine the effect of Ago2 ablation on mitochondrial function, we evaluated the expression of mitochondria structural proteins. Mitochondrial shape and structure are maintained by two opposing forces, i.e., fission and fusion. Fission is controlled by the dynamin-related protein 1 (Drp1) and the mitochondrial fission 1 (Fis1) protein, and fusion is controlled by mitofusin (Mfn)[31]. In Ago2-KO mice, the expression of Drp1 and Fis1 was significantly higher than those in WT mice (Fig. 5D-E). In contrast, MFN in Ago2-KO mice was significantly decreased compared with that in WT mice. Furthermore, under diabetic condition, we observed an obvious increased Drp1 and Fis1 and decreased Mfn expression in WT+HFD/STZ mice, and Ago2-KO+HFD/STZ further enhanced the changes of protein expression (Fig. 5D-E). Ultrastructural analysis of SCs in sciatic nerves showed that, compared to WT mice, Ago2-KO mice displayed dilatated mitochondria and vacuoles (Fig. 5F). Moreover, Ago2-KO mice had significant augmentations of swollen mitochondria with expanded matrix space, and fragmented or disorganized cristae in myelinated and non-myelinated axons of sciatic nerves (Fig. 5G-H).

Ago2 regulates RAGE/NF-κB pathway via altering its bound miRNAs in peripheral nerves

We next investigated the mechanism underlying the effect of Ago2 knockout on non-myelinating and myelinating axonal damage in diabetic mice with neuropathy. Using the Ago2 immunoprecipitation approach which detected the miRNAs with their target genes that bind to Ago2[36,373], we performed Ago2-based RNA immunoprecipitation (RIP) in combination with miRNA sequencing in sciatic nerve tissues from WT and Ago2-KO mice. We found that the miR-206 was one of the most downregulated Ago2-bound miRNAs in Ago2-KO mice compared with WT mice (Fig. 6A). A significant reduction of Ago2-bound miR-206 was further validated using qRT-PCR (Fig. 6C). TargetScan algorithm prediction demonstrated that miR-206 targets the receptor for advanced glycation end product (RAGE) (Fig. 6B). Western blot assay revealed that the expression of RAGE in the sciatic nerve tissues of Ago2-KO mice was significantly higher than that in WT mice (Fig. 6D-E), which was negatively correlated with the downregulation of miR-206 in the sciatic nerve tissues of Ago2-KO mice. In the sciatic nerves of Ago2-KO+HFD/STZ mice, RAGE expression was further increased compared with non-diabetic Ago2-KO mice and WT+HFD/STZ mice (Fig. 6D-E).

AGE induces ROS generation via the RAGE/NF-κB pathway[384]. We found the ROS level in the sciatic nerve of Ago2-KO mice was significantly increased compared with that in WT mice (Fig. 6H). In WT+HFD/STZ mice, ROS content was higher than in non-diabetic WT mice, and Ago2-KO further increased the content of ROS compared with WT+HFD/STZ mice (Fig. 6H). We also observed the increased expression of NF-κB p65 and caspase-3 in Ago2-KO mice (Fig. 6D-E), which was positively correlated with the elevated ROS levels. Double immunofluorescence staining of TUNEL and RFP in sciatic nerves demonstrated that Ago2-KO markedly increased the apoptosis of SCs (Fig. 6F-G). These data suggest that Ago2-KO-induced alteration of miRNA profile led to apoptosis via the RAGE signaling.

To investigate the effect of miR-206 on SC function, we transfected the cultured SCs with a miR-206 inhibitor. Western blot assay demonstrated that knockdown of miR-206 significantly increased the expression of target RAGE and the downstream pNF-κB and Caspase-3 compared with the negative control group (Fig. 6I-J). Moreover, loss of miR-206 induced mitochondrial dysfunction, manifested as decreased $\Delta\psi m$ and deregulated expression of Mfn and Fis1, and increased ROS production in SCs (Fig. 6K-L). These results provide strong evidence that the miR-206 cluster contributes to the regulation of mitochondrial function in Ago2-KO SCs.

Discussion

In the present study, we investigated the involvement of Ago2 in the development of peripheral neuropathy. Our data demonstrated that conditional ablation of Ago2 in PLP lineage SCs of non-diabetic mice induced peripheral neuropathy, measured by mechanical and thermal allodynia, and nerve conduction velocity. Ago2-KO in SCs induced demyelination and loss of axons. In the HFD/STZ type 2 diabetes model, depletion of Ago2 accelerated and worsened DPN. Ablation of Ago2 in SCs resulted in alteration of miRNA profiles and mitochondrial dysfunction in sciatic nerves. These novel findings

provide insights into the roles of SC Ago2 in maintaining peripheral nerve function and in development of the pathogenesis of DPN.

Recent studies demonstrated that miRNAs are key regulators in the maintenance of homeostasis in the PNS. The ablation of Ago2 induced a global reduction of miRNAs, thereby allowing us to investigate the role of SC miRNAs that may associate with the dysregulation of cell cycle, differentiation, and cell survival. Previous studies found miRNAs, including miRNA-9, −23b, −27, −29, −144, and −222 et al., directly or indirectly affected the transcription factors for SC differentiation and myelination[39–417]. In our study, Ago2-KO in SCs induced failed myelin maintenance, followed by the degeneration of myelinated axons. When diabetes was induced by HFD/STZ, axonal demyelination was exacerbated in Ago2-KO mice, and thus accelerated the development of DPN. These data provide evidence supporting that: 1) Ago2-miRNAs complexes play essential roles in maintaining myelin integrity, and 2) SC dysfunction has direct effects on neurons, resulting in axon structure disruption and impaired nerve conduction velocity.

Our data (Fig. 2b) showed Ago2 KO reduced the percentage of large (>8 um) nerve fibers, indicating that Aα motor fibers may be affected and leading to the reduction of MCV. At the early stage of DPN in patients, sensory peripheral nerves are primarily affected, but at the later stage, DPN also affects motor nerve fibers in the patients with reduction of conductivity velocity of motor peripheral nerves. Thus, DPN induced by Ago2 KO may represent patients with a later stage of DPN.

Clinical and experimental studies have shown that sex and age play an important role in occurrence and progression of DPN. We have demonstrated that male animals develop a greater extent of diabetes-induced peripheral neurovascular dysfunction than females[21]. Thus, in the present study, we use male mice to investigate the effect of Ago2 deletion in SCs on DPN. Investigation of the effect of ablation of SC Ago2 on DPN in female mice is warranted for future study.

Mitochondria are critical regulators in the development and maintenance of peripheral nerves[8,9,12]. Axonal regeneration requires high consumption of mitochondrially derived ATP[427, 38]. Mitochondrial dysfunction can impair the cellular energy metabolism, leading to cell death, inflammation and neurodegeneration[8]. Structurally or functionally abnormal mitochondria are preferentially found in SCs in the peripheral nerves of both human patients with diabetes and in animal models of diabetes[12]. Chronic exposure of cells to high levels of glucose causes dramatic changes in the mitochondrial proteome, which lead to decreased mitochondrial metabolic activity in various cell types, including SCs. These results support the premise that SC mitochondria are involved in the development of DPN. The ablation of Ago2 was demonstrated to disturb energy metabolism in the pathogenesis of obesity[439]. Ago2 was found associated with mitochondrial genome in relation to cell metabolism[40]. Roger et al. found that the Ago2 insufficiency in brown adipose tissue of rats decreased mitochondrial respiration[41]. Our data demonstrated that in vivo depletion of Ago2 in PLP lineage SCs led to abnormality of mitochondrial structure, mitochondrial DNA loss, and significantly lowered mitochondrial potential, permeability and ATP levels, as well as increased ROS production in sciatic nerve tissues. These data suggest that Ago2 alteration

in SCs is involved in mitochondrial defects and oxidative stress, leading to a substantial reduction of axons and peripheral neuropathy resembling those caused by diabetes.

The Ago2-miRNA complex is involved in the regulation of mRNA translation within mitochondria[442]. Using Ago2-RIP analysis, we revealed that deletion of Ago2 in PLP-lineage SCs decreased sets of mRNAs and Ago2-bound miRNAs that are known to regulate oxidative phosphorylation and mitochondrial function. Amongst them, the miR-206, which potentially targets RAGE, was identified to be highly downregulated. miR-206 beneficially promotes nerve-muscle interactions in response to injury of motor neurons[455]. In the PNS, RAGE is predominantly expressed in SCs and endothelial cells and is upregulated in diabetes[466]. It is well-documented that the advanced glycation end products (AGEs)-RAGE axis has deleterious effects on mitochondrial respiration and oxidative phosphorylation, triggering increased ROS production and oxidative stress[477]. Our data along with the noted studies suggest that downregulation of Ago2 in peripheral nerve tissues reduces the targeting efficacy of bound miR-206 against RAGE, consequently leading to the activation of RAGE and mitochondrial dysfunction. We acknowledge that Ago2 affects many miRNAs that may be involved in mediating and facilitating the axonal damage by diabetes. Our study thus delineates a novel role of Ago2-dependent miRNA-mRNA silencing in the regulation of SC mitochondrial function and axonal regeneration.

In the diabetic context, excessive production of AGEs interacts with RAGE, stimulating inflammatory reactions and the production of cytosolic ROS, thereby accelerating the progression of DPN[488]. In addition, RAGE triggers intracellular signaling pathways that culminate in the activation of the transcription factor NF-κB and subsequent transcription of many genes, including endothelin-1, tissue factor, TNF-α, and interleukin-1[466]. The admission of the antagonist scavenging RAGE ligand could prevent the increase of NF-κB and ameliorate the loss of thermal perception in mice with DPN[499]. Our data demonstrated that Ago2-KO decreased miR-206 which increased RAGE. RAGE activates the synthesis of NF-κB p65 and therefore enhances the dysfunction and apoptosis of SCs. Taken together, these observations suggest that the enhancement of the interaction of miR-206 with RAGE is a novel therapeutic strategy for the treatment of DPN in diabetes. A limitation is that due to technical challenges, we are unable to isolate and culture highly pure primary SCs and neurons from adult WT and Ago-KO mice, and whether the dysregulations of miR-206, ROS production, NFkB, RAGE, etc, are limited to axons or SCs of the PNS is unclear.

SC-axon interaction is implicated in the maintenance of peripheral nerve function[50]. It is not surprising that impaired SCs lead to altered axonal properties. Our group previously reported SC-exosomes promote neurite outgrowth of DRG neurons in vitro and in vivo[51]. Schwann cells assist DRG neurons in locally synthesizing proteins in axons and dendrites by way of exosomal miRNAs[502]. In the present study, we observed that Ago2-KO SCs were unable to form normal Remak bundles of unmyelinated small-caliber axons, which is consistent with sensory deficits. The DRG neurons isolated from Ago2-KO mice showed a significantly reduced axonal growth rate compared to those isolated from wild-type mice. A potential mechanism is that Ago2 ablation in SCs alters the cargos of SC exosomes, which counteracts their protective effect on DRG neurons in non-cell autonomous manner. In addition, neurotrophic factors play important roles for supporting axon function in the

PNS. It is likely that the Ago2-KO in SCs alters the trophic support to DRG neurons and consequently induces axonal damage, which warrants investigation.

Conclusion

In summary, our results show that the absence of Ago2 in SCs induced mitochondrial dysfunction via the RAGE/NF-κB signaling pathway. Ago2 downregulation in SCs strongly influenced the activity of miRNAs and exacerbated the demyelination and neurodegeneration of sciatic nerves, which lead to peripheral neuropathy in diabetic and non-diabetic mice. Our data suggest that the Ago2-miRNA complex could potentially be a promising therapeutic target in the treatment of DPN.

Acknowledgments

We thank Julie Landschoot-Ward, Qinge Lu, and Sutapa Santra for the immunostaining, and Min Wei and William Golembieski for transgenic mouse breeding and genotyping.

Funding:

This work was supported by U.S. National Institutes of Health (NIH) National Institute of Diabetes and Digestive and Kidney Diseases (NIDDK) Diacomp Program grant 21AU4165 (to X.S.L) and American Heart/Stroke Association Grant 18IPA34170331 (to X.S.L.). The authors declare no conflicts of interest.

Reference

1. Boyle JP, Thompson TJ, Gregg EW, Barker LE & Williamson DF Projection of the year 2050 burden of diabetes in the US adult population: dynamic modeling of incidence, mortality, and prediabetes prevalence. Popul Health Metr 8, 29, doi:10.1186/1478-7954-8-29 (2010). [PubMed: 20969750]
2. Finnerup NB, Sindrup SH & Jensen TS The evidence for pharmacological treatment of neuropathic pain. Pain 150, 573–581, doi:10.1016/j.pain.2010.06.019 (2010). [PubMed: 20705215]
3. St Onge EL & Miller SA Pain associated with diabetic peripheral neuropathy: a review of available treatments. P T 33, 166–176 (2008). [PubMed: 19750158]
4. Goncalves NP et al. Schwann cell interactions with axons and microvessels in diabetic neuropathy. Nat Rev Neurol 13, 135–147, doi:10.1038/nrneurol.2016.201 (2017). [PubMed: 28134254]
5. Smith RS & Koles ZJ Myelinated nerve fibers: computed effect of myelin thickness on conduction velocity. Am J Physiol 219, 1256–1258, doi:10.1152/ajplegacy.1970.219.5.1256 (1970). [PubMed: 5473105]
6. Goncalves NP et al. Schwann cell p75 neurotrophin receptor modulates small fiber degeneration in diabetic neuropathy. Glia 68, 2725–2743, doi:10.1002/glia.23881 (2020). [PubMed: 32658363]
7. Jessen KR, Mirsky R. & Lloyd AC Schwann Cells: Development and Role in Nerve Repair. Cold Spring Harbor perspectives in biology 7, a020487, doi:10.1101/cshperspect.a020487 (2015).
8. Viader A. et al. Aberrant Schwann cell lipid metabolism linked to mitochondrial deficits leads to axon degeneration and neuropathy. Neuron 77, 886–898, doi:10.1016/j.neuron.2013.01.012 (2013). [PubMed: 23473319]
9. Ino D. & Iino M. Schwann cell mitochondria as key regulators in the development and maintenance of peripheral nerve axons. Cellular and molecular life sciences : CMLS 74, 827–835, doi:10.1007/s00018-016-2364-1 (2017). [PubMed: 27638763]
10. Schroder JM Neuropathy associated with mitochondrial disorders. Brain Pathol 3, 177–190, doi:10.1111/j.1750-3639.1993.tb00742.x (1993). [PubMed: 8293179]
11. Hosseini A. & Abdollahi M. Diabetic neuropathy and oxidative stress: therapeutic perspectives. Oxid Med Cell Longev 2013, 168039, doi:10.1155/2013/168039 (2013).

12. Viader A. et al. Schwann cell mitochondrial metabolism supports long-term axonal survival and peripheral nerve function. J Neurosci 31, 10128–10140, doi:10.1523/jneurosci.0884-11.2011 (2011). [PubMed: 21752989]
13. Simeoli R. & Fierabracci A. Insights into the Role of MicroRNAs in the Onset and Development of Diabetic Neuropathy. Int J Mol Sci 20, doi:10.3390/ijms20184627 (2019).
14. Fan B, Chopp M, Zhang ZG & Liu XS Emerging Roles of microRNAs as Biomarkers and Therapeutic Targets for Diabetic Neuropathy. Front Neurol 11, 558758, doi:10.3389/fneur.2020.558758 (2020).
15. Sohn EJ & Park HT MicroRNA Mediated Regulation of Schwann Cell Migration and Proliferation in Peripheral Nerve Injury. Biomed Res Int 2018, 8198365, doi:10.1155/2018/8198365 (2018).
16. Peters L. & Meister G. Argonaute proteins: mediators of RNA silencing. Mol Cell 26, 611–623, doi:10.1016/j.molcel.2007.05.001 (2007). [PubMed: 17560368]
17. Arroyo JD et al. Argonaute2 complexes carry a population of circulating microRNAs independent of vesicles in human plasma. Proc Natl Acad Sci U S A 108, 5003–5008, doi:10.1073/pnas.1019055108 (2011). [PubMed: 21383194]
18. Ye Z, Jin H. & Qian Q. Argonaute 2: A Novel Rising Star in Cancer Research. J Cancer 6, 877–882, doi:10.7150/jca.11735 (2015). [PubMed: 26284139]
19. Karginov FV & Hannon GJ Remodeling of Ago2-mRNA interactions upon cellular stress reflects miRNA complementarity and correlates with altered translation rates. Genes Dev 27, 1624–1632, doi:10.1101/gad.215939.113 (2013). [PubMed: 23824327]
20. Fan B. et al. Mesenchymal stromal cell-derived exosomes ameliorate peripheral neuropathy in a mouse model of diabetes. Diabetologia 63, 431–443, doi:10.1007/s00125-019-05043-0 (2020). [PubMed: 31740984]
21. Fan B. et al. Influence of Sex on Cognition and Peripheral Neurovascular Function in Diabetic Mice. Frontiers in neuroscience 12, 795, doi:10.3389/fnins.2018.00795 (2018). [PubMed: 30429771]
22. Chaplan SR, Bach FW, Pogrel JW, Chung JM & Yaksh TL Quantitative assessment of tactile allodynia in the rat paw. Journal of neuroscience methods 53, 55–63 (1994). [PubMed: 7990513]
23. Fan B, Chopp M, Zhang ZG & Liu XS Treatment of diabetic peripheral neuropathy with engineered mesenchymal stromal cell-derived exosomes enriched with microRNA-146a provide amplified therapeutic efficacy. Exp Neurol 341, 113694, doi:10.1016/j.expneurol.2021.113694 (2021).
24. Liu XS et al. MicroRNA-146a Mimics Reduce the Peripheral Neuropathy in Type II Diabetic Mice. Diabetes, doi:10.2337/db16-1182 (2017).
25. Liu XS et al. MicroRNA-146a Mimics Reduce the Peripheral Neuropathy in Type 2 Diabetic Mice. Diabetes 66, 3111–3121, doi:10.2337/db16-1182 (2017). [PubMed: 28899883]
26. Wang L. et al. Sildenafil ameliorates long term peripheral neuropathy in type II diabetic mice. PLoS One 10, e0118134, doi:10.1371/journal.pone.0118134 (2015).
27. Wang L. et al. Phosphodiesterase-5 is a therapeutic target for peripheral neuropathy in diabetic mice. Neuroscience 193, 399–410, doi:10.1016/j.neuroscience.2011.07.039 (2011). [PubMed: 21820491]
28. Xu HP, Gou L. & Dong HW Study glial cell heterogeneity influence on axon growth using a new coculture method. Journal of visualized experiments : JoVE, doi:10.3791/2111 (2010).
29. Zhang Y. et al. MicroRNAs in the axon locally mediate the effects of chondroitin sulfate proteoglycans and cGMP on axonal growth. Developmental neurobiology 75, 1402–1419, doi:10.1002/dneu.22292 (2015). [PubMed: 25788427]
30. Aguayo AJ, Charron L. & Bray GM Potential of Schwann cells from unmyelinated nerves to produce myelin: a quantitative ultrastructural and radiographic study. J Neurocytol 5, 565–573, doi:10.1007/BF01175570 (1976). [PubMed: 978232]
31. Chomiak T. & Hu B. What is the optimal value of the g-ratio for myelinated fibers in the rat CNS? A theoretical approach. PLoS One 4, e7754, doi:10.1371/journal.pone.0007754 (2009). [PubMed: 19915661]
32. Nebuchennykh M, Loseth S, Lindal S. & Mellgren SI The value of skin biopsy with recording of intraepidermal nerve fiber density and quantitative sensory testing in the assessment of small

fiber involvement in patients with different causes of polyneuropathy. J Neurol 256, 1067–1075, doi:10.1007/s00415-009-5065-y (2009). [PubMed: 19252773]

33. Jacobson RD, Virág I. & Skene JH A protein associated with axon growth, GAP-43, is widely distributed and developmentally regulated in rat CNS. J Neurosci 6, 1843–1855, doi:10.1523/jneurosci.06-06-01843.1986 (1986). [PubMed: 3712014]
34. Jia L. et al. MicroRNA 146a locally mediates distal axonal growth of dorsal root ganglia neurons under high glucose and sildenafil conditions. Neuroscience 329, 43–53, doi:10.1016/j.neuroscience.2016.05.005 (2016). [PubMed: 27167084]
35. Patti ME & Corvera S. The role of mitochondria in the pathogenesis of type 2 diabetes. Endocr Rev 31, 364–395, doi:10.1210/er.2009-0027 (2010). [PubMed: 20156986]
36. Liu XS et al. Identification of miRNomes associated with adult neurogenesis after stroke using Argonaute 2-based RNA sequencing. RNA biology 14, 488–499, doi:10.1080/15476286.2016.1196320 (2017). [PubMed: 27315491]
37. Ahadi A, Sablok G. & Hutvagner G. miRTar2GO: a novel rule-based model learning method for cell line specific microRNA target prediction that integrates Ago2 CLIP-Seq and validated microRNA-target interaction data. Nucleic acids research 45, e42, doi:10.1093/nar/gkw1185 (2017). [PubMed: 27903911]
38. Piras S. et al. RAGE Expression and ROS Generation in Neurons: Differentiation versus Damage. Oxid Med Cell Longev 2016, 9348651, doi:10.1155/2016/9348651 (2016).
39. Bremer J. et al. Ablation of Dicer from murine Schwann cells increases their proliferation while blocking myelination. PloS one 5, e12450, doi:10.1371/journal.pone.0012450 (2010).
40. Verrier JD, Semple-Rowland S, Madorsky I, Papin JE & Notterpek L. Reduction of Dicer impairs Schwann cell differentiation and myelination. Journal of neuroscience research 88, 2558–2568, doi:10.1002/jnr.22418 (2010). [PubMed: 20648646]
41. Pereira JA et al. Dicer in Schwann cells is required for myelination and axonal integrity. The Journal of neuroscience : the official journal of the Society for Neuroscience 30, 6763–6775, doi:10.1523/jneurosci.0801-10.2010 (2010). [PubMed: 20463238]
42. Baloh RH Mitochondrial dynamics and peripheral neuropathy. The Neuroscientist : a review journal bringing neurobiology, neurology and psychiatry 14, 12–18, doi:10.1177/1073858407307354 (2008). [PubMed: 17911220]
43. Zhang C. et al. Hepatic Ago2-mediated RNA silencing controls energy metabolism linked to AMPK activation and obesity-associated pathophysiology. Nat Commun 9, 3658, doi:10.1038/s41467-018-05870-6 (2018). [PubMed: 30201950]
44. Bandiera S, Hanein S, Lyonnet S. & Henrion-Caude A. Mitochondria as novel players of the cellular RNA interference. J Biol Chem 286, le19, doi:10.1074/jbc.L111.240259 (2011).
45. Williams AH et al. MicroRNA-206 delays ALS progression and promotes regeneration of neuromuscular synapses in mice. Science 326, 1549–1554, doi:10.1126/science.1181046 (2009). [PubMed: 20007902]
46. Wada R. & Yagihashi S. Role of advanced glycation end products and their receptors in development of diabetic neuropathy. Ann N Y Acad Sci 1043, 598–604, doi:10.1196/annals.1338.067 (2005). [PubMed: 16037282]
47. Ramasamy R, Yan SF & Schmidt AM Receptor for AGE (RAGE): signaling mechanisms in the pathogenesis of diabetes and its complications. Ann N Y Acad Sci 1243, 88–102, doi:10.1111/j.1749-6632.2011.06320.x (2011). [PubMed: 22211895]
48. Sugimoto K, Yasujima M. & Yagihashi S. Role of advanced glycation end products in diabetic neuropathy. Curr Pharm Des 14, 953–961, doi:10.2174/138161208784139774 (2008). [PubMed: 18473845]
49. Bierhaus A. et al. Loss of pain perception in diabetes is dependent on a receptor of the immunoglobulin superfamily. J Clin Invest 114, 1741–1751, doi:10.1172/jci18058 (2004). [PubMed: 15599399]
50. Xia B. et al. Mechanical stimulation of Schwann cells promote peripheral nerve regeneration via extracellular vesicle-mediated transfer of microRNA 23b-3p. Theranostics 10, 8974–8995, doi:10.7150/thno.44912 (2020). [PubMed: 32802175]

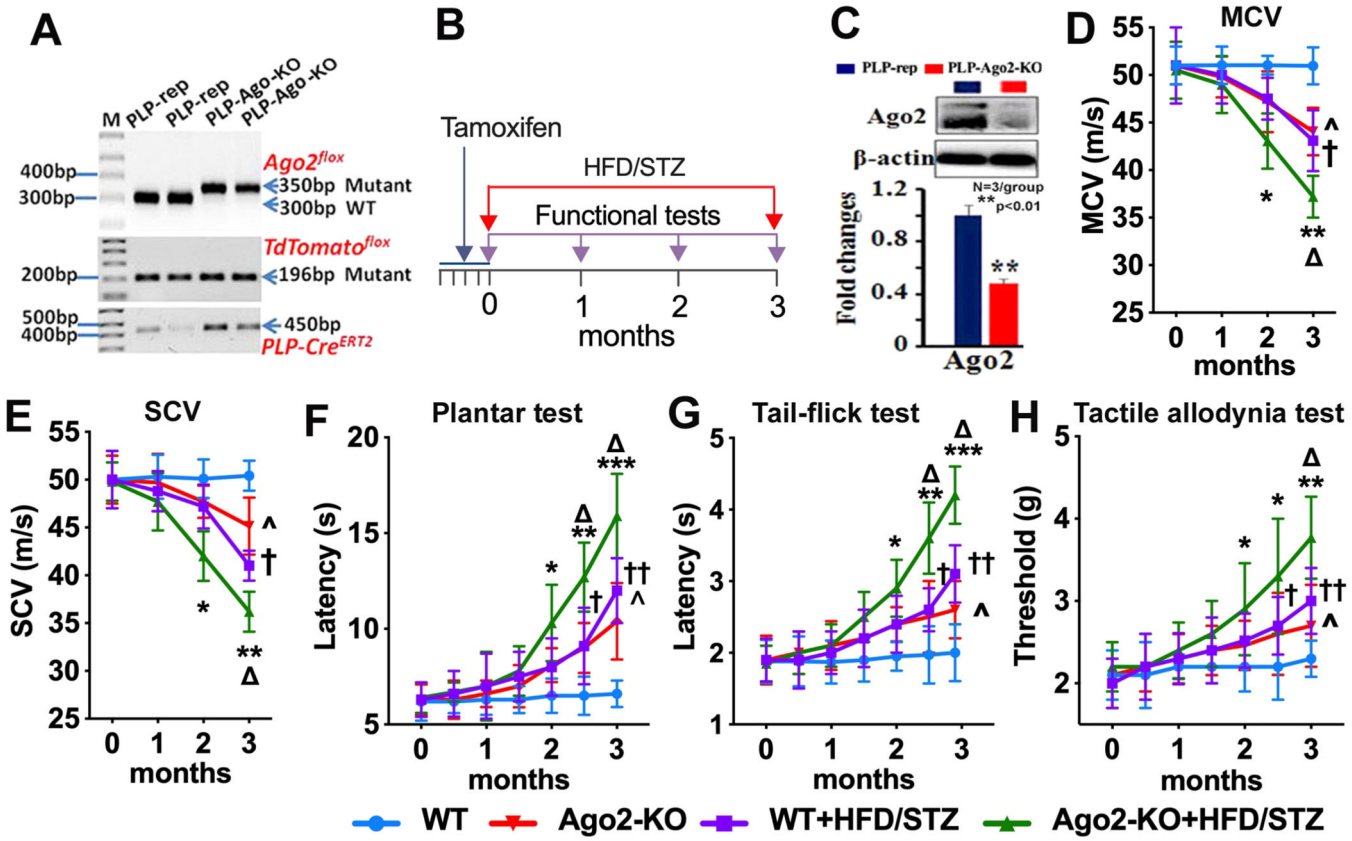

Figure 1.

Ablation of Ago2 in SCs accelerates the progression of DPN. Panel A shows the genotyping of PLP-Cre^{ERT2};Ago2$^{-/-}$;Tom (PLP-Ago-KO) and WT (PLP-rep) mice. (B) The schematic diagram shows the timeline of treatment and tests. Panel C shows levels of Ago2 protein in sciatic nerve isolated from PLP-rep and PLP-Ago2-KO mice. M: DNA ladder marker. (D-H) SC specific Ago2-KO significantly decreased motor (MCV, D) and sensory nerve conduction (SCV, E), and increased the threshold to thermal (F, plantar test; G, tail-flick test) and mechanical (H, tactile allodynia test) stimuli compared with WT mice. N = 12/group. ^p<0.05 WT vs Ago2-KO. †p<0.05, ††p<0.01 WT vs WT+HFD/STZ. *p<0.05, ** p<0.01, *** p<0.001 Ago2-KO+HFD/STZ vs WT. Δ p<0.05 Ago2-KO+HFD/STZ vs WT+HFD/STZ.

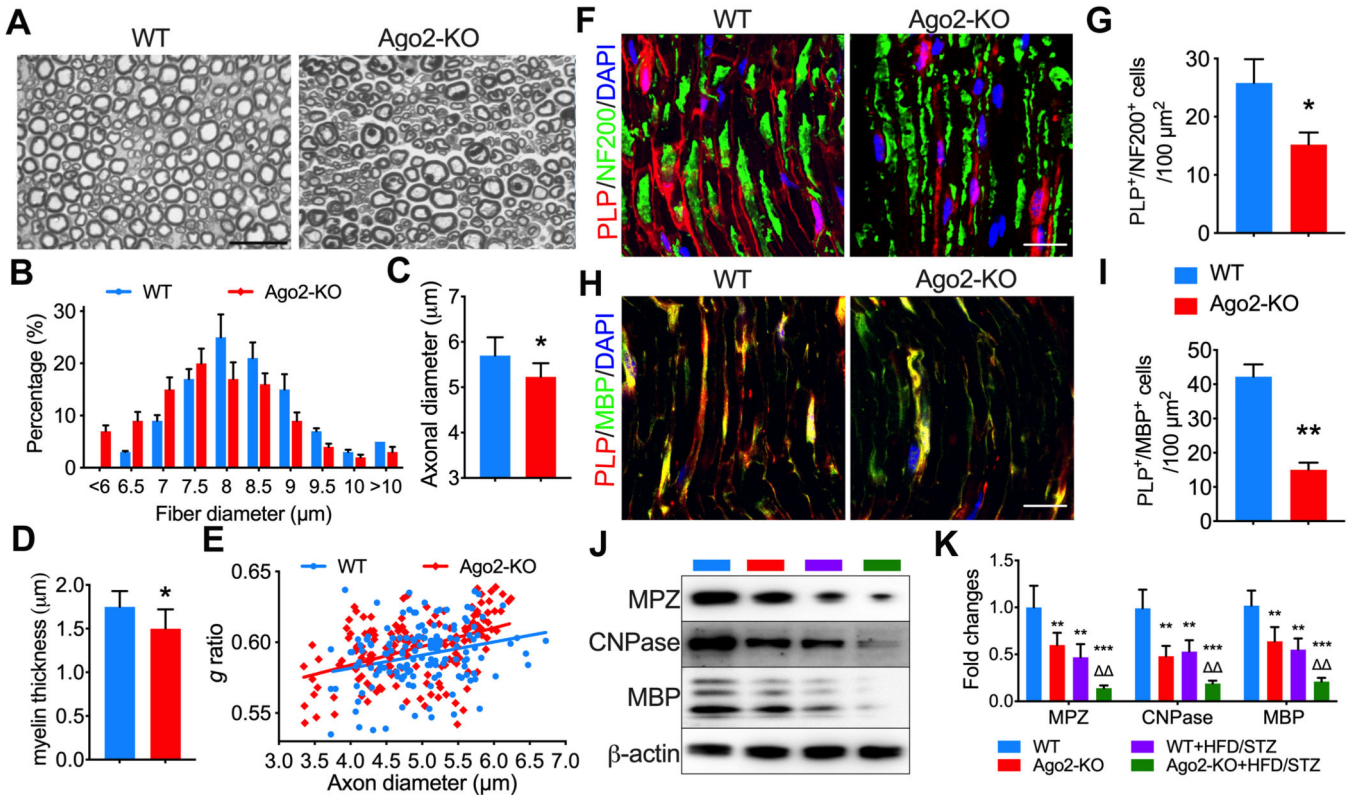

Figure 2.

Ago2 deletion in SCs induced demyelination and loss of axons. (A) Semi-thin toluidine blue stained cross sections of sciatic nerves. Bar = 20μm. (B) Histograms showing the frequency distribution of the diameters of myelinated fibers. Ago2-KO mice exhibited decreased axonal diameter (C) and myelin thickness (D). (E) Scatter plot shows g ratios of individual fibers as a function of the respective axon diameter. (F-I) Representative immunofluorescence images and quantitative data of coexpressed PLP^+/RFP^+ (red) with $NF200^+$ (green) or MBP^+ (green) cells in sciatic nerves. The yellow color in the merged images indicates co-localization of PLP^+/RFP^+ and $NF200^+$ or MBP^+ cells. Nuclei are counterstained with DAPI (blue). Bar=20μm. N=6. (J-K) Western blot analysis and quantitative data of relative expression levels of MPZ, CNPase and MBP in sciatic nerve from all groups. N=3. *p<0.05, **p<0.01, ***p<0.001 vs WT. $^{\Delta\Delta}$p<0.01 Ago2-KO+HFD/STZ vs WT+HFD/STZ.

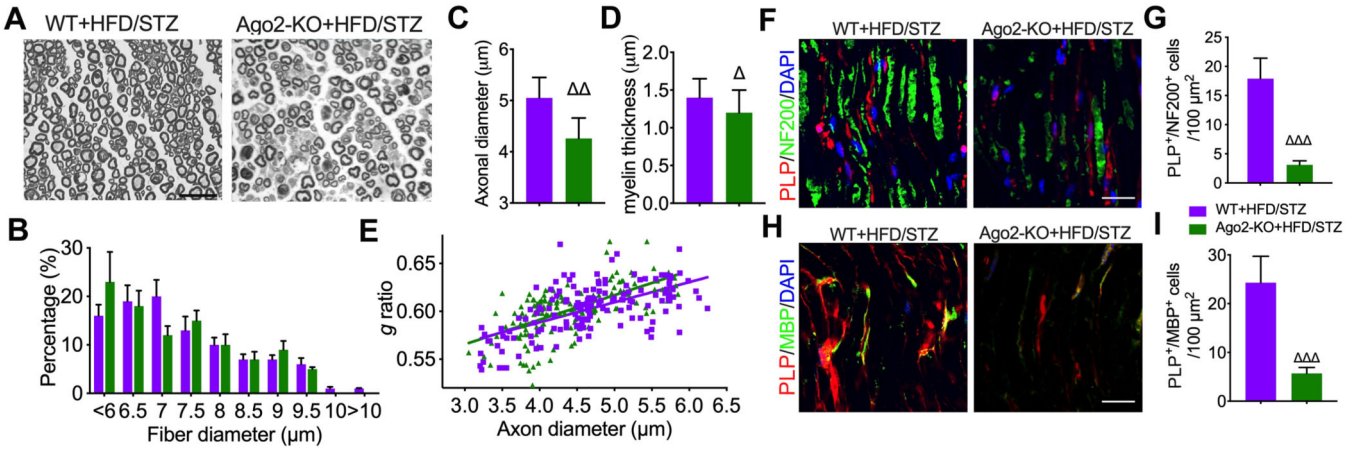

Figure 3.

Ago2 deletion in SCs exacerbated demyelination in diabetic mice. A: Semi-thin toluidine blue stained cross sections of sciatic nerves. Bar = 20μm. B: Histograms show the frequency distribution of the diameters of myelinated fibers. Ago2-KO mice exhibited decreased axonal diameter (C) and myelin thickness (D). E: Scatter plot shows g ratios of individual fibers as a function of the respective axon diameter. F-I: Representative immunofluorescence images and quantitative data of co-localization of PLP^+/RFP^+ (red) with $NF200^+$ (green) or MBP^+ (green) cells in sciatic nerves. The yellow color in the merged images indicates co-localization of PLP^+/RFP^+ with $NF200^+$ or MBP^+ cells. Nuclei are counterstained with DAPI (blue). Bar=20μm. N=6. $^{\Delta}p<0.05$, $^{\Delta\Delta}p<0.01$, $^{\Delta\Delta\Delta}p<0.001$ Ago2-KO+HFD/STZ vs WT+HFD/STZ.

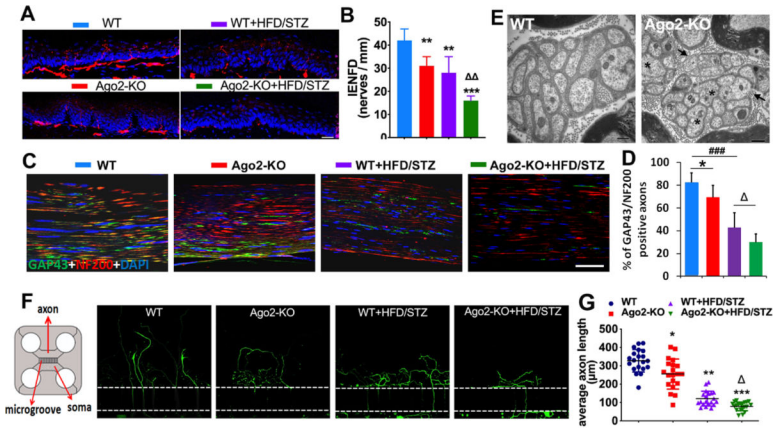

Figure 4.

A-B: PGP9.5 staining IENF in hind paw plantar skin. The density of IENF was decreased in groups induced by HFD/STZ. Ago2-KO enhanced diabetes-induced loss of IENF. Bar=20μm. N=6. Representative images (C) and quantitative data (D) of $GAP43^{+}/NF200^{+}$ axons from sciatic nerves of Ago2-KO or WT mice induced by HFD/STZ. Bar=50μm. E: Representative transmission electron microscopy (TEM) images of sciatic nerves. Bar=400nm. F-G: Ago2-KO in Schwann cells suppressed DRG neuron axonal outgrowth. F (Left): Schematic of microfluidic device. Representative images (F, right) and quantitative data (G) of axonal growth. DRG neurons were isolated and cultured in chambers. Axonal length was measured for each group at 72h later. *p<0.05, **p<0.01, ***p<0.001 vs WT. $^{\Delta}$p<0.05, $^{\Delta\Delta}$p<0.01 Ago2-KO+HFD/STZ vs WT+HFD/STZ.

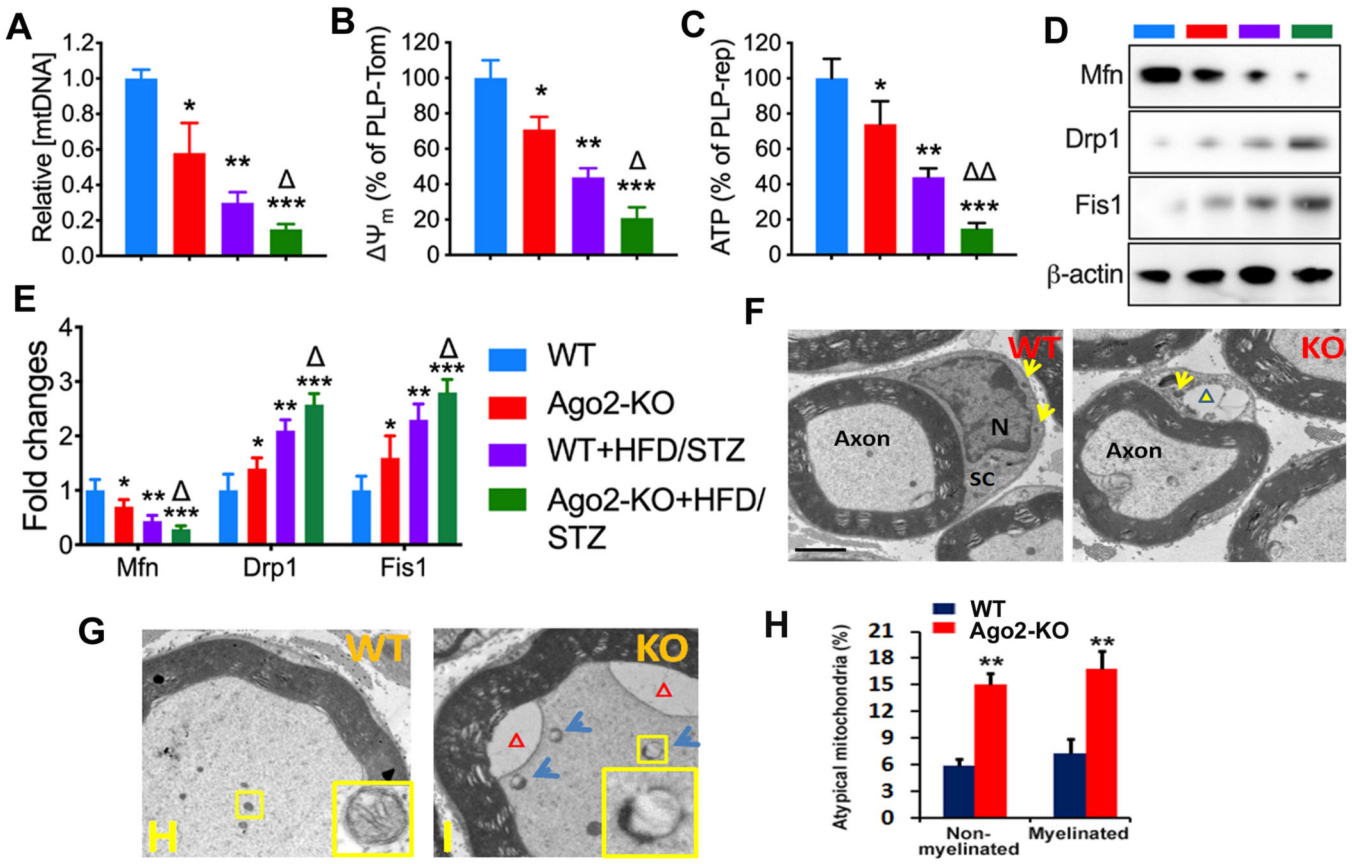

Figure. 5.

Mitochondrial DNA (mtDNA) (A), the mitochondrial membrane potential (Δψm) (B), and ATP content (C) in the sciatic nerves harvested from Ago2-KO or WT mice treated/non-treated with HFD/STZ. D-E: Western blot analysis of MFN, DRP1, and FIS1 in sciatic nerves harvested from Ago2-KO or reporter mice treated/non-treated with HFD/STZ. N=3/group. *p<0.05, **p<0.01, ***p<0.001 vs WT. $^{\Delta}$p<0.05, $^{\Delta\Delta}$p<0.01 Ago2-KO+HFD/STZ vs WT+HFD/STZ. (F) Electron micrograph showing dilatation mitochondria and vacuoles within Schwann cells (SCs) in Ago2-KO compared to WT mice. (G, H) Representative ultrastructure micrographs and quantification of the atypical mitochondria in Ago2-KO or WT mice. N: nucleus. Arrows: mitochondria. Triangle: vacuoles. Scale bar: 1μm.

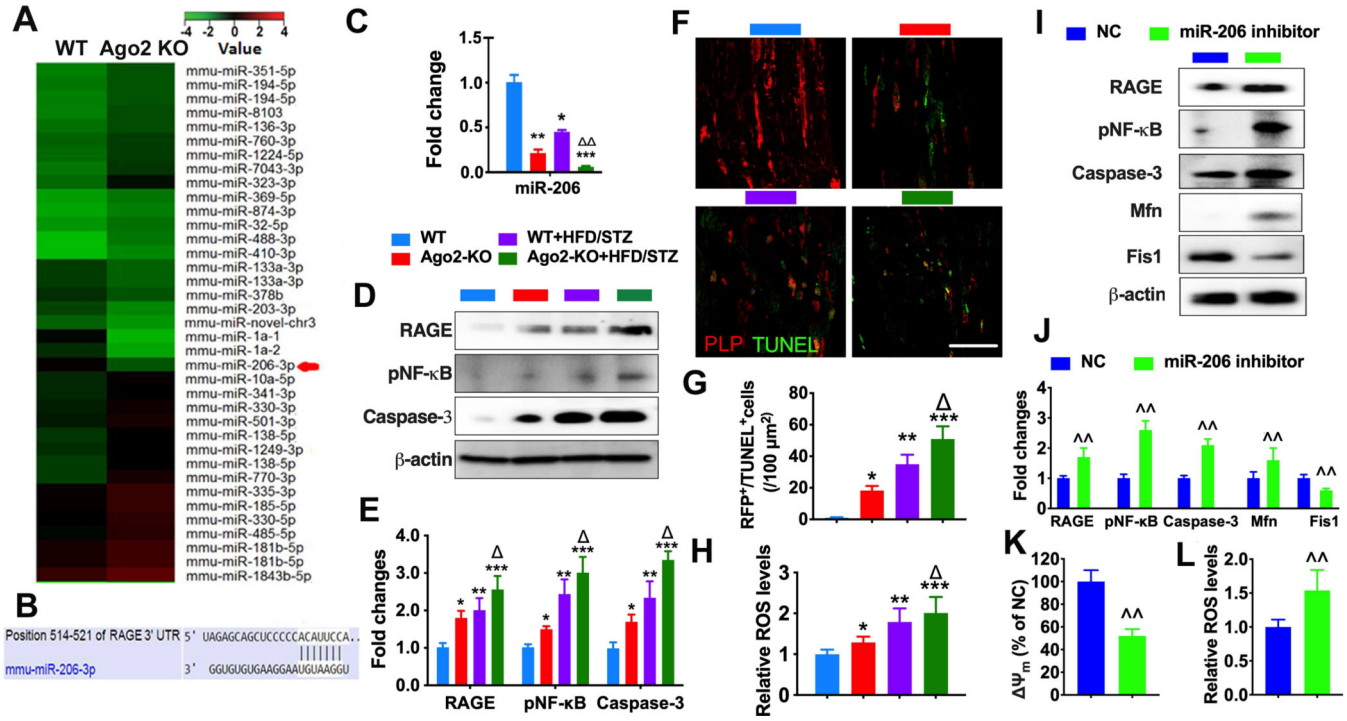

Figure. 6.

A: Representative heat map of miRNA sequence analysis in the sciatic nerves from Ago2-KO or WT mice. B: Predicted miR-206 binding site in the 3'-UTR of RAGE. C: QRT-PCR data show the level of miR-206 in the sciatic nerves harvested from Ago2-KO or WT mice treated/non-treated with HFD/STZ. D-E: Western blot analysis of RAGE, NF-κB and Caspase-3 in sciatic nerves harvested from all groups. F-G: TUNEL assay of the sciatic nerves harvested from Ago2-KO or WT mice treated/non-treated with HFD/STZ. N=6/group. Bar=50μm. *p<0.05, **p<0.01, ***p<0.001 vs WT. $^{\Delta}$p<0.05, $^{\Delta\Delta}$p<0.01 Ago2-KO+HFD/STZ vs WT+HFD/STZ. H: The content of ROS in the sciatic nerves. I-J: Western blot analysis of RAGE, NF-κB, Caspase-3, Mfn, and Fis1 in SCs transfected with miR-206 inhibitor or negative control (NC). K: The mitochondrial membrane potential (Δψm) of SCs transfected with miR-206 inhibitor or NC L: The content of ROS in SCs transfected with miR-206 inhibitor or NC. N=3/group. ^^ p<0.01 vs NC.

Table 1

Effect of Ago2 ablation in SCs on morphometric changes of myelinated sciatic nerves

Property	WT	WT+HFD/STZ	Ago2-KO	Ago-KO+HFD/STZ
Fiber diameter(μm)	8.94±0.27	7.96±0.33 ###	8.55±0.32	7.20±0.31 †††, ∓ ∓
Axon diameter(μm)	5.85±0.27	4.83±0.27 #	5.15±0.20 *	4.48±0.20 †††, ∓
myelin thickness(μm)	1.86±0.10	1.56±0.08	1.48±0.21 *	1.36±0.07 †
g ratio	0.58±0.01	0.61±0.01 ###	0.60±0.01 *	0.62±0.01 †††, ∓ ∓ ∓

# p<0.05

p<0.001 WT vs WT+HFD/SZT

† p<0.05

††† p<0.001 Ago-KO vs Ago-KO+HFD/STZ

* p<0.05, WT vs Ago-KO

∓ p<0.05

∓ ∓ p<0.01

∓ ∓ ∓ p<0.001 WT+HFD/SZT vs Ago-KO+HFD/STZ. Bar= 25μm